In vivo optical imaging of human lymphoma xenograft using a library-derived peptidomimetic against α4β1 integrin

Li Peng, Ruiwu Liu, Mirela Andrei, Wenwu Xiao, and Kit S. Lam

Division of Hematology and Oncology, Department of Internal Medicine, University of California Davis Cancer Center, Sacramento, California

Abstract

Increasing literature suggests that cell adhesion molecule α4β1 integrin plays a pivotal role in autoimmune diseases and cancer development. Noninvasive visualization of α4β1 integrin *in vivo* will facilitate the understanding of its involvement in disease progression and development of targeted therapies. Due to the lack of high-affinity targeting ligands, molecular imaging of α4β1 integrin is much less explored than that of αvβ3 and αvβ5 integrins. We have recently reported using the one bead–one compound combinatorial library method to identify a peptidomimetic, LLP2A, that preferentially binds to activated α4β1 integrin. Here, we described the use of LLP2A-Cy5.5 conjugate as an *in vivo* optical imaging probe in a human lymphoma xenograft model. This univalent LLP2A-Cy5.5 conjugate retained the binding activity and specificity to α4β1 integrin as shown by cell binding assays using α4β1-positive Molt-4 T-leukemia cells. The subcutaneous Molt-4 tumor was clearly visualized from 1 to 24 h after tail vein injection of the conjugate. Direct imaging and confocal microscopic examination of excised tumors and organs confirmed the accumulation of LLP2A in tumors and revealed very little or no uptake in normal organs except for lymph nodes. Kidney uptake was high when the whole organ was scanned but it was negative when examined microscopically, suggesting that LLP2A bound to the renal tubules loosely. Tumor uptake of LLP2A-Cy5.5 conjugate was blocked by excess unlabeled LLP2A. This study showed that the combinatorial chemical library-derived peptidomimetic LLP2A can be easily developed into an optical imaging probe for noninvasively monitoring of activated α4β1 integrin *in vivo*. [Mol Cancer Ther 2008;7(2):432–7]

Introduction

Integrins are heterodimeric transmembrane proteins crucial for cell-cell, cell-matrix, and cell-pathogen interactions and play important roles in autoimmune diseases, cancer metastasis, tumor angiogenesis, and viral infections (1–3). Based on the physiologic conditions, they may exist in the resting or activated states (1, 4). Imaging of various integrins at different states can provide useful information about the receptor status during disease progression and may provide important clues for the development of specific therapeutics for various diseases. Antibodies, cyclic RGD peptides, and peptidomimetics against αvβ3 integrin have been intensely studied for tumor imaging (5–10) and for therapeutic blockage of tumor angiogenesis (11–13). It is well known that α4β1 integrin is important in autoimmune diseases and inflammation (14, 15). There is increasing evidence that α4β1 integrin is also involved in tumor growth, angiogenesis, and metastasis (16–25). Integrin α4β1 is found to express on leukemias, lymphomas, melanomas, and sarcomas (16). It facilitates tumor cell extravasation (16, 17), prevents apoptosis of malignant B-chronic lymphocytic leukemia cells (19), plays important roles in the drug resistance of both multiple myeloma (20) and acute myelogenous leukemia (21), and is an excellent therapeutic target for malignant lymphoid cancers (24, 26). In addition, α4β1 is found to express on spouting tumor vessels but not on quiescent endothelial cells (23, 25). Despite of its importance, α4β1 integrin is much less explored in *in vivo* imaging due to the lack of high-affinity and high-specificity targeting ligands for the receptor.

Small peptides and peptidomimetics have been widely pursued for targeting because of their fast clearance and better tumor penetration over high molecular weight protein-based targeting agents, such as monoclonal antibodies. Furthermore, they are less likely than antibodies to bind to the reticuloendothelial system. Both radiolabeled or near IR (NIR) fluorochrome–conjugated derivatives of regulatory peptides (such as somatostatin and vasoactive intestinal peptide) and RGD peptides have been used to noninvasively visualize and quantify their counter receptors *in vivo* for tumor detection and study of tumor progression (10, 27–29). We recently reported the discovery of a high-affinity peptidomimetic ligand, LLP2A, that preferentially binds to activated α4β1 integrin. This ligand was identified from highly focused one bead–one compound combinatorial libraries (24). We have also shown that

Received 8/20/07; revised 11/5/07; accepted 12/20/07.

Grant support: NIH R33 CA86364, NIH R33 CA99136, NCI NCDDG U19 CA113298, and NSF CHE-0302122. The 500-MHz nuclear magnetic resonance spectrometer was purchased in part with the grant NSF 9724412.

The costs of publication of this article were defrayed in part by the payment of page charges. This article must therefore be hereby marked *advertisement* in accordance with 18 U.S.C. Section 1734 solely to indicate this fact.

Requests for reprints: Kit S. Lam, Division of Hematology and Oncology, University of California Davis Cancer Center, 4501 X Street, Sacramento, CA 95817. Phone: 916-734-8012; Fax: 916-734-7946.
E-mail: Kit.Lam@ucdmc.ucdavis.edu

doi:10.1158/1535-7163.MCT-07-0575

LLP2A, when biotinylated and complexed with Alexa680-streptavidin conjugate to form a tetravalent molecule (molecular weight, ~60,000 Da), was able to target human lymphoma xenograft in nude mice with high sensitivity and specificity. Kidney was the only organ with high uptake. However, similar kidney uptake was also observed with Alexa680-streptavidin alone without any targeting ligand (24). Whereas it is convenient to use streptavidin-fluorochrome as a contrast agent to evaluate *in vivo* targeting potential of tumor-targeting ligands, it has several limitations: (*a*) the final conjugate is protein based and relatively large, and therefore, it loses the advantage of small ligands with rapid clearance and rapid tumor penetration; (*b*) streptavidin is immunogenic and therefore will not be very useful for human applications; (*c*) streptavidin binds to normal kidneys; and (*d*) tetravalency and therefore high avidity may be desirable in some applications but not others.

In this study, we reported on the design and synthesis of a small (2,295 Da) univalent LLP2A-Cy5.5 conjugate and the successful use of it for *in vivo* imaging of $\alpha4\beta1$-positive lymphoma xenografts in nude mice. NIR fluorochromes, such as Cy5.5, allow the imaging of deeper tissues due to their properties of high penetration and low tissue absorption and scattering (28, 30, 31) and have been used by many investigators in optical imaging of different types of tumors (9, 32, 33).

Materials and Methods

Materials

RPMI medium, sodium pyruvate solution, and sodium bicarbonate solution were purchased from American Type Culture Collection. FCS was purchased from Omega Scientific. Rink amide MBHA resin (loading 0.65 mmol/g) was purchased from GL Biochem. Fmoc-Lys[1-(4,4-dimethyl-2,6-dioxocyclohex-1-ylidene)ethyl]-OH were purchased from EMD Biosciences. Cy5.5-NHS dye was purchased from Amersham Bioscience Co. All other chemical reagents were purchased from Aldrich.

Synthesis of LLP2A-Cy5.5

The detail synthesis of LLP2A-Cy5.5 is shown in the Supplementary material.[1] Briefly, Fmoc-Lys[1-(4,4-dimethyl-2,6-dioxocyclohex-1-ylidene)ethyl] was first coupled to the amino of rink amide MBHA resin. Then, Fmoc was deprotected; two polyethylene glycol–like short linker (34) were coupled to the α-amino of lysine sequentially, followed by assembly of LLP2A as previously described (24). The 1-(4,4-dimethyl-2,6-dioxocyclohex-1-ylidene)ethyl protecting group of the ε-amino of lysine was removed with 2% NH_2NH_2, followed by coupling of Cy5.5-NHS. The final product was cleaved off the beads using trifluoroacetic acid mixture, followed by high-performance liquid chromatography purification. The identity was verified by MALDI-MS.

[1] Supplementary data for this article are available at Molecular Cancer Therapeutics Online (http://mct.aacrjournals.org/).

Cell Adhesion Assays

Molt-4 cells were obtained from American Type Culture Collection. The binding affinity (IC_{50}) of LLP2A-Cy5.5 was characterized in a Molt-4 cell adhesion assay by inhibiting the $\alpha4\beta1$-mediated cell adhesion to CS-1 peptides, which is the binding motif of fibronectin to $\alpha4\beta1$ integrin. Ninety-six–well plates were coated with 1 μg/mL neutravidin, followed by the biotin-conjugated CS-1 peptide synthesized, as previously described (24) after washing. The wells were blocked with 1% bovine serum albumin in PBS for 1 h. Molt-4 cells with serial dilutions of tested compounds in 100 μL binding buffer (TBS, 1mmol/L Mn^{2+}) were added and allowed to bind for 30 min. Unbound cells were removed by gentle washing. Bound cells were fixed with 3.7% formaldehyde and stained with 0.1% crystal violet. The dye was dissolved in 1% SDS and recorded on a 96-well plate reader (SAFIRE, TECAN) at 570 nm. IC_{50} data were calculated from inhibition curves resulting from the concentration-dependent inhibition.

Tumor Xenografts

Animal procedures were done in compliance with institutional guidelines and according to protocol no. 04-11527 approved by the Animal Use and Care Administrative Advisory Committee in University of California Davis. Female athymic nude mice (nu/nu) were obtained from Harlan at 4 to 6 weeks of age. Molt-4 cells (~5×10^6 cells) were injected s.c. into one side of the shoulder of animals. When tumors measured ~0.5 to 0.8 cm in diameter, the tumor-bearing mice were subject to *in vivo* imaging.

Confocal Microscopy

For cell staining assays, cells were incubated with the LLP2A-Cy5.5 (1 nmol/L) for 30 min at 37°C in TBS buffer (1 mmol/L Mg^{2+}). An excess of LLP2A (100 μmol/L) was added for blocking in the presence of 1 nmol/L of LLP2A-Cy5.5. Then cells were washed thrice with TBS and examined with a Zeiss LSM510 confocal microscope. For confocal microscopic analysis of tissues, we excised tumors and organs 6 h after tail vein injection of 0.5 nmol LLP2A-Cy5.5 and froze them with liquid nitrogen. Frozen tissues were cryosectioned into sections 7-μm thick and fixed with acetone. Slides were rehydrated in PBS for 5 min and stained with 4′,6-diamidino-2-phenylindole to visualize tissue morphology. We mounted slides with coverslips and examined them with a spectral deconvolution Olympus FV1000 laser scanning confocal microscope. The images of Cy5.5 signals were acquired with a tunable filter automatically stepping in 10-nm increments from 580 to 750 nm and generated through separating autofluorescence and Cy5.5 spectra by applying normal spectral deconvolution algorithms provided by the FV1000 software.

Animal Imaging

In vivo NIR fluorescence imaging experiments were done on nu/nu mice bearing Molt-4 tumors using Kodak multimodal imaging system IS2000MM (Kodak) equipped with an excitation bandpass filter at 625 nm and an emission at 700 nm. Mice were given injection via tail vein with different amounts of LLP2A-Cy5.5, 2 nmol ($n = 4$) or 0.5 nmol ($n = 4$). For blocking experiment, mice ($n = 3$)

received 200 nmol LLP2A 30 min before the injection of 0.5 nmol LLP2A-Cy5.5. Animals were anesthetized using i.p. injection of pentobarbital (60 mg/kg) and imaged at various time points postinjection. Exposure time was 30 s per image. Images were analyzed using the imaging station IS2000MM provided software (Kodak 1D Image Analysis Software; Kodak).

After *in vivo* imaging, animals that received 0.5 nmol LLP2A-Cy5.5 were euthanized by CO_2 overdose 6 h after injection. Tumors, organs, and muscle tissue were excised and imaged with the Kodak imaging system as described above.

Data Processing and Statistics

All the data are given as mean ± SD of *n* independent measurements. For determination of tumor contrast, mean fluorescence intensities of the tumor area and the normal tissue area were calculated by means of the region-of-interest function using Kodak 1D Image Analysis Software (Kodak).

Results

Synthesis and Characterization of LLP2A-Cy5.5

LLP2A-Cy5.5 was obtained as dark blue powder. The chemical structure of LLP2A-Cy5.5 is shown in Fig. 1. The identity of the compound was confirmed by MALDI-TOF MS, MS (m/z): 2,295 (M^+). The purity of the final product as shown in analytic high-performance liquid chromatography was over 90% (254 nm).

Specificity of LLP2A-Cy5.5 to α4β1 integrin

To determine whether Cy5.5 conjugation had any effect on the binding characteristics of LLP2A, we measured the IC_{50} of LLP2A-Cy5.5 in a competitive Molt-4 cell adhesion assay. LLP2A-Cy5.5 blocked the interaction between α4β1 integrin on Molt-4 cells and CS-1 peptide of fibronectin, which is the natural ligand for α4β1 integrin, in a concentration-dependent manner. The IC_{50} of LLP2A-Cy5.5 was determined to be 13 ± 5 pmol/L.

To evaluate the binding specificity of LLP2A-Cy5.5 conjugates to α4β1 integrin, we test them with Molt-4 leukemia cells that express α4β1 integrin and α4-transfected K562 (chronic myelogenous leukemia) cells. After incubating these cells with LLP2A-Cy5.5, fluorescence signals were observed on both α4β1-expressing Molt-4 and α4-transfected K562 cells (Fig. 2A and B); no staining was observed on untransfected parental K562 cells, which express α5β1 integrin (Fig. 2C). The staining of LLP2A-Cy5.5 was completely abolished by the presence of an excess of unlabeled LLP2A (Fig. 2D and E). This study shows that the LLP2A-Cy5.5 conjugate retained the binding activity and specificity to its receptor α4β1 integrin.

In vivo NIR Fluorescence Imaging

To investigate the targeting efficiency of LLP2A-Cy5.5 conjugate *in vivo*, mice with subcutaneously grown Molt-4 tumors were injected with 2 nmol LLP2A-Cy5.5 through the tail vein. The whole animal became fluorescent immediately after injection; substantial contrast between tumors and normal tissue was observed from 1 to 24 h postinjection (Fig. 3A).

To validate the specificity of *in vivo* targeting, we did a blocking experiment with unlabeled LLP2A. Control mice received 0.5 nmol LLP2A-Cy5.5 conjugate, and animals in blocking group were injected with 200 nmol of unlabeled LLP2A 30 min before the injection of 0.5 nmol LLP2A-Cy5.5. As shown in Fig. 3B, unlabeled LLP2A successfully blocked uptake of LLP2A-Cy5.5 into the tumor.

To determine organ distribution of the injected LLP2A-Cy5.5 conjugate, we excised the tumor and organs 6 h postinjection and did *ex vivo* gross imaging. It confirmed that LLP2A-Cy5.5 conjugate was accumulated primarily in the Molt-4 tumors (Fig. 3C). LLP2A retention in other normal organs was low, with little uptake in lymph node and skin, except for the kidneys which showed high fluorescence signals (Fig. 3C).

We also examined organ distribution of the conjugate with confocal microscope using spectral deconvolution algorithms to separate autofluorescence of tissues and Cy5.5 signals. The study clearly showed that LLP2A-Cy5.5 conjugate uptake was high in the lymphoma xenograft but none was detected in other normal organs except for the lymph node (Fig. 4). Although there was high fluorescent signal in the gross signal of the entire kidney, no Cy5.5 signal was detected microscopically (Fig. 4). Together, these results showed that univalent LLP2A targets to α4β1-expressing tumors *in vivo* in a xenograft model with high specificity.

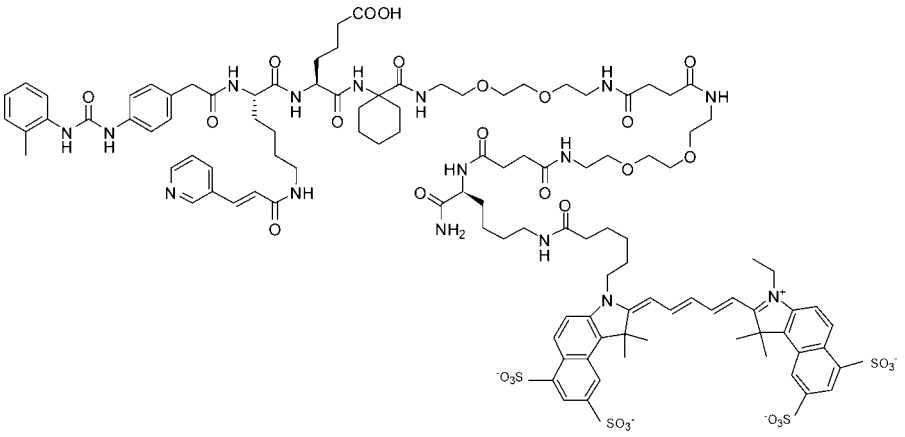

Figure 1. Chemical structure of LLP2A-Cy5.5.

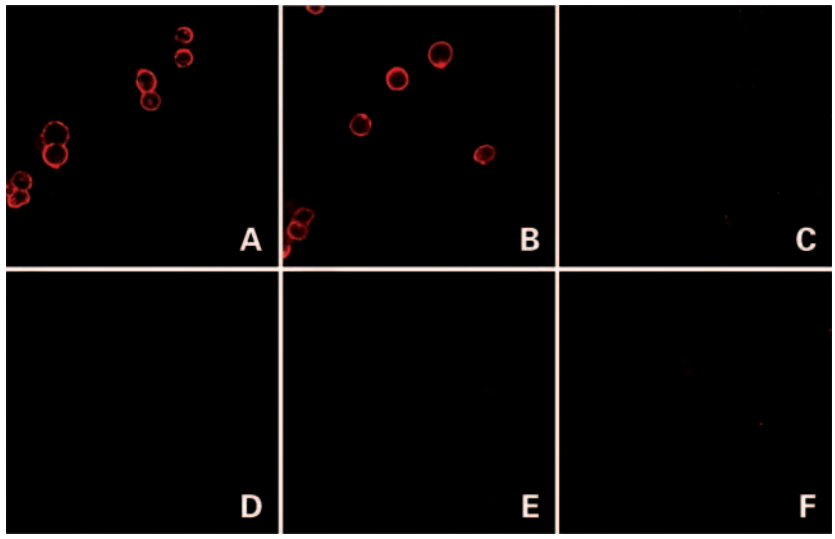

Figure 2. Specific binding of LLP2A-Cy5.5 to $\alpha4\beta1$ integrin. Confocal microscopy images of Molt-4 (**A** and **D**), $\alpha4$-transfected K562 (**B** and **E**), and parental K562 (**C** and **F**) cells incubated for 1 h at 37°C in the presence of 1 nmol/L LLP2A-Cy5.5 with (**D – F**) or without (**A – C**) blocking dose of unlabeled LLP2A (100 μmol/L). Note that only $\alpha4\beta1$-expressing Molt-4 (**A**) and $\alpha4$-transfected K562 cells (**B**) efficiently bind the conjugate, and excess LLP2A completely blocked the NIR fluorescence signals (**D** and **E**), demonstrating the high specificity of LLP2A-Cy5.5.

Discussion

The emergence of molecular imaging has a significant effect on basic research and potentially on clinical care in the future. Development of high-affinity targeting probes is one of the key prerequisites for imaging of specific molecular targets in living systems. With the advances in genomic and proteomics, many potential therapeutic targets have been identified. Discovery of novel imaging agents against these targets enables *in vivo* molecular target assessment and, therefore, facilitates the understanding of their roles in disease progression and the development of targeted therapeutics. Targeting ligands must have the ability to reach the targets with sufficient concentration and retention time to be detectable *in vivo*. An ideal molecular imaging agent should have the following properties: high-affinity and specificity against targeted molecules, metabolically stable, rapid excretion, and very low nonspecific binding.

High-affinity cancer targeting ligands can be developed rationally based on the structural information of natural ligands and targeted receptors, or they can be developed through screening random and focused combinatorial libraries (35, 36). In the last few years, we have successfully used the one bead–one compound combinatorial library approach to identify several cancer-specific targeting ligands (24, 35–38). We previously reported that a one bead–one compound combinatorial library-derived $\alpha4\beta1$ integrin targeting peptidomimetic (LLP2A), when conjugated to fluorochrome-labeled streptavidin in a tetravalent form, could image lymphoma xenograft with high specificity (24). Here, we show that LLP2A, when

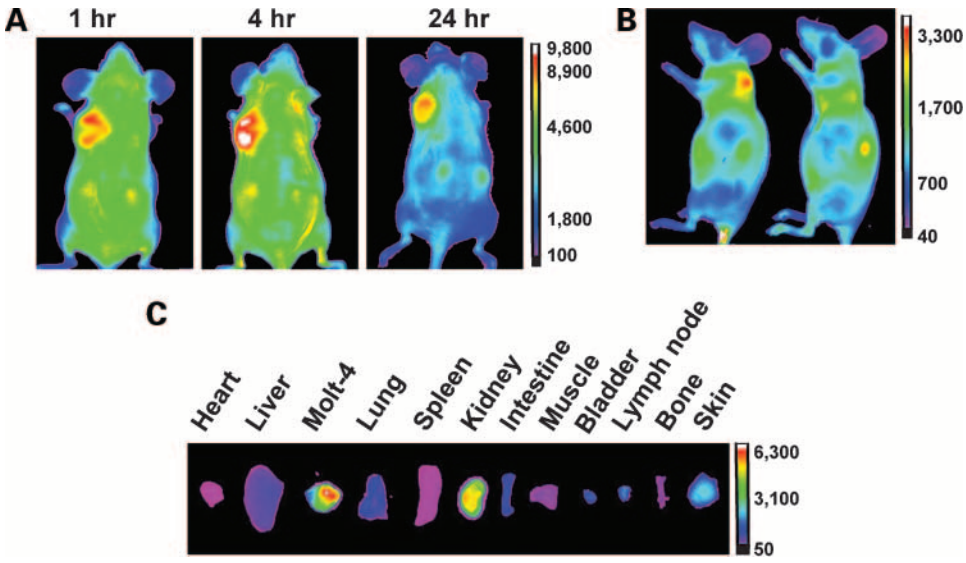

Figure 3. NIR fluorescence imaging of subcutaneous Molt-4 tumor-bearing mice. The LLP2A-Cy5.5 was given at a dose of 2 nmol (**A**) or 0.5 nmol (**B** and **C**) per mouse via tail vein. All NIR fluorescence images were acquired with 30 s exposure time at different time points postinjection. **A,** *in vivo* fluorescence images of subcutaneous Molt-4 tumor-bearing mice received 2 nmol LLP2A-Cy5.5 conjugates. Fluorescence signals from Cy5.5 were pseudocolored. **B,** *in vivo* NIR fluorescence images of mice at 3 h after injection of 0.5 nmol LLP2A-Cy5.5 without blocking (*left*) or with blocking (*right*) by injecting 200 nmol LLP2A 30 min before probe administration. **C,** *ex vivo* images of excised tumors and organs 6 h after injection of 0.5 nmol LLP2A-Cy5.5.

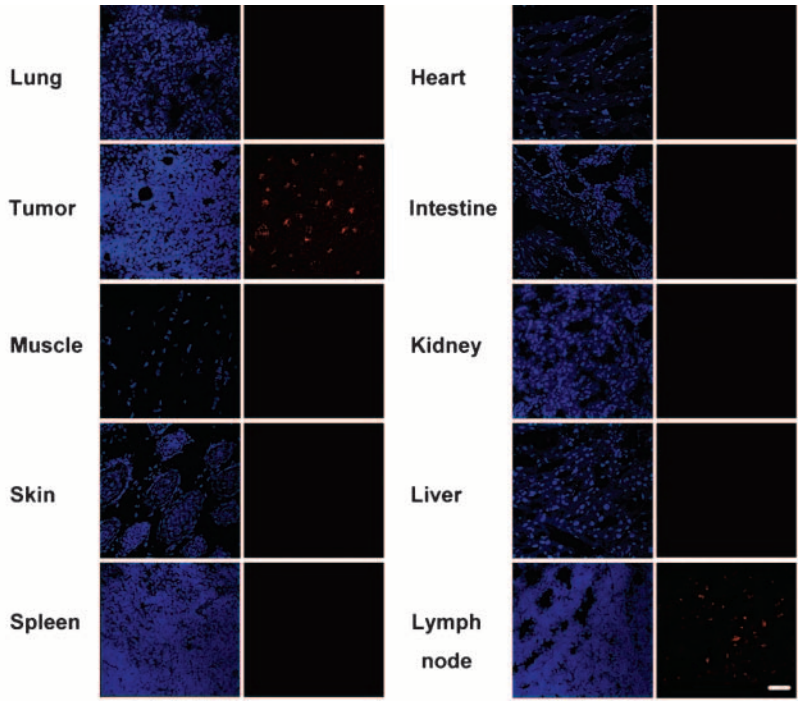

Figure 4. Confocal microscopic analysis of tumor uptake and organ distribution of LLP2A-Cy5.5. Tumors and organs were frozen immediately after *ex vivo* imaging of mice (as shown in Fig. 3C) received 0.5 nmol LLP2A-Cy5.5 6 h postinjection. Tissue morphology was visualized by staining nuclei with 4′,6-diamidino-2-phenylindole (*blue*). The signals of Cy5.5 (*red*) were acquired with a tunable filter automatically stepping in 10-nm increments from 580 to 750 nm. Images of pure Cy5.5 signals were generated through separating autofluorescence and Cy5.5 spectra using spectral deconvolution algorithms. *Scale bar,* 30 μm.

conjugated to Cy5.5 via a hydrophilic linker as a small molecule univalent conjugate, still retained its *in vitro* lymphoma cell–binding and *in vivo* tumor-targeting characteristics.

Incubation of Molt-4 leukemia cells and α4-transfected K562 cells with LLP2A-Cy5.5 resulted in strong fluorescence signals on cell membrane, and the staining was diminished by adding excess unlabeled LLP2A. No fluorescence was seen on α4β1-negative K562 cells upon incubation. The conjugate also indicated integrin-specific tumor accumulation because unlabeled LLP2A blocked tumor uptake *in vivo*.

Direct *ex vivo* imaging and microscopic analysis of excised tissues and organs confirmed the specific localization of LLP2A-Cy5.5 at tumors and revealed its organ distribution. Strong fluorescence signals in tumors were observed both in *ex vivo* imaging and confocal microscopic examination. In kidneys, *ex vivo* images of the whole organ was high, but there was no detectable fluorescence in the kidney microscopic sections, which suggested that the probe retention in kidneys might be caused by loosely localized probes in renal tubular structure and the probes came off during the slide preparation procedures for confocal microscopy, such as cryosectioning and rehydration. The uptake in other organs was low, as shown in both *ex vivo* organ imaging and microscopic analysis, except for lymph nodes, which showed some fluorescence signals through confocal microscopic examination. The low fluorescence signal of lymph nodes in *ex vivo* imaging was due to its much smaller tissue size comparing to other organs for imaging, as direct organ imaging collected all signals of the whole tissue mass. On the other hand, confocal microscopic analysis examined all organs using the same thickness slides and with the same size of field of view. The uptake of LLP2A-Cy5.5 in lymph nodes might be caused by the binding of LLP2A to activated lymphocytes.

In summary, we have described the successful NIR imaging of α4β1-positive tumor, such as lymphoma using the combinatorial library-derived peptidomimetic LLP2A through direct conjugation with Cy5.5 dye. The study has further confirmed the usage of one bead–one compound combinatorial chemistry approach to identify novel targeting ligands as potential molecular imaging agents. The promising optical imaging data obtained in this study have paved ways for the development of univalent LLP2A-radiometal chelate conjugate in our laboratory for more quantitative radioimaging and radiotherapeutic studies in nude mice, canine, and human patients. Preliminary data suggests that radiolabeled univalent LLP2A exhibits high tumor-specific uptake in xenograft models. In addition, work is under way in our laboratory to conjugate LLP2A to doxorubicin for targeted therapeutic studies *in vivo*.

Acknowledgments

We thank Dr. A. Lehman, Dr. C. Pan, and Dr. X. Wang for editorial assistance.

References

1. Hynes RO. Integrins: bidirectional, allosteric signaling machines. Cell 2002;110:673–7.

2. Martin KH, Slack JK, Boerner SA, Martin CC, Parsons JT. Integrin connections map: to infinity and beyond. Science 2002;296:1652–3.

3. Hwang R, Varner J. The role of integrins in tumor angiogenesis. Hematol Oncol Clin North Am 2004;18:991–1006.

4. Shimaoka M, Takagi J, Springer TA. Conformational regulation of integrin structure and function. Annu Rev Biophys Biomol Struct 2002;31:485–516.

5. Sivolapenko GB, Skarlos D, Pectasides D, et al. Imaging of metastatic

melanoma utilising a technetium-99m labelled RGD-containing synthetic peptide. Eur J Nucl Med 1998;25:1383 – 9.

6. Haubner R, Wester HJ, Weber WA, et al. Noninvasive imaging of $\alpha(v)\beta3$ integrin expression using 18F-labeled RGD-containing glycopeptide and positron emission tomography. Cancer Res 2001;61:1781 – 5.

7. Janssen ML, Oyen WJ, Dijkgraaf I, et al. Tumor targeting with radiolabeled $\alpha(v)\beta(3)$ integrin binding peptides in a nude mouse model. Cancer Res 2002;62:6146 – 51.

8. Su ZF, He J, Rusckowski M, Hnatowich DJ. *In vitro* cell studies of technetium-99m labeled RGD-HYNIC peptide, a comparison of tricine and EDDA as co-ligands. Nucl Med Biol 2003;30:141 – 9.

9. Chen X, Conti PS, Moats RA. *In vivo* near-infrared fluorescence imaging of integrin $\alpha v\beta3$ in brain tumor xenografts. Cancer Res 2004;64: 8009 – 14.

10. Chen X. Multimodality imaging of tumor integrin $\alpha v\beta3$ expression. Mini Rev Med Chem 2006;6:227 – 34.

11. Shimaoka M, Springer TA. Therapeutic antagonists and conformational regulation of integrin function. Nat Rev Drug Discov 2003;2:703 – 16.

12. Jin H, Varner J. Integrins: roles in cancer development and as treatment targets. Br J Cancer 2004;90:561 – 5.

13. Cai W, Chen X. Anti-angiogenic cancer therapy based on integrin $\alpha v\beta3$ antagonism. Anticancer Agents Med Chem 2006;6:407 – 28.

14. Lin KC, Castro AC. Very late antigen 4 (VLA4) antagonists as anti-inflammatory agents. Curr Opin Chem Biol 1998;2:453 – 7.

15. Yusuf-Makagiansar H, Anderson ME, Yakovleva TV, Murray JS, Siahaan TJ. Inhibition of LFA-1/ICAM-1 and VLA-4/VCAM-1 as a therapeutic approach to inflammation and autoimmune diseases. Med Res Rev 2002;22:146 – 67.

16. Holzmann B, Gosslar U, Bittner M. $\alpha4$ integrins and tumor metastasis. Curr Top Microbiol Immunol 1998;231:125 – 41.

17. Vincent AM, Cawley JC, Burthem J. Integrin function in chronic lymphocytic leukemia. Blood 1996;87:4780 – 8.

18. Marco RA, Diaz-Montero CM, Wygant JN, Kleinerman ES, McIntyre BW. $\alpha4$ integrin increases anoikis of human osteosarcoma cells. J Cell Biochem 2003;88:1038 – 47.

19. de la Fuente MT, Casanova B, Garcia-Gila M, Silva A, Garcia-Pardo A. Fibronectin interaction with $\alpha4\beta1$ integrin prevents apoptosis in B cell chronic lymphocytic leukemia: correlation with Bcl-2 and Bax. Leukemia 1999;13:266 – 74.

20. Damiano JS, Dalton WS. Integrin-mediated drug resistance in multiple myeloma. Leuk Lymphoma 2000;38:71 – 81.

21. Matsunaga T, Takemoto N, Sato T, et al. Interaction between leukemic-cell VLA-4 and stromal fibronectin is a decisive factor for minimal residual disease of acute myelogenous leukemia. Nat Med 2003;9:1158 – 65.

22. Olson DL, Burkly LC, Leone DR, Dolinski BM, Lobb RR. Anti-$\alpha4$ integrin monoclonal antibody inhibits multiple myeloma growth in a murine model. Mol Cancer Ther 2005;4:91 – 9.

23. Garmy-Susini B, Jin H, Zhu Y, Sung RJ, Hwang R, Varner J. Integrin $\alpha4\beta1$-VCAM-1-mediated adhesion between endothelial and mural cells is required for blood vessel maturation. J Clin Invest 2005;115: 1542 – 51.

24. Peng L, Liu R, Marik J, Wang X, Takada Y, Lam KS. Combinatorial chemistry identifies high-affinity peptidomimetics against $\alpha4\beta1$ integrin for *in vivo* tumor imaging. Nat Chem Biol 2006;2:381 – 9.

25. Jin H, Su J, Garmy-Susini B, Kleeman J, Varner J. Integrin $\alpha4\beta1$ promotes monocyte trafficking and angiogenesis in tumors. Cancer Res 2006;66:2146 – 52.

26. Park SI, Manat R, Vikstrom B, Amro N, Song LW, Lam KS. The use of one-bead one-compound combinatorial library method to identify peptide ligands for α-4-β-1 integrin receptor in non-Hodgkin's lymphoma. Lett Pept Sci 2002;8:171 – 8.

27. O'Byrne KJ, Carney DN. Radiolabelled somatostatin analogue scintigraphy in oncology. Anticancer Drugs 1996;7:33 – 44.

28. Becker A, Hessenius C, Licha K, et al. Receptor-targeted optical imaging of tumors with near-infrared fluorescent ligands. Nat Biotechnol 2001;19:327 – 31.

29. Bhargava S, Licha K, Knaute T, et al. A complete substitutional analysis of VIP for better tumor imaging properties. J Mol Recognit 2002; 15:145 – 53.

30. Ntziachristos V, Bremer C, Weissleder R. Fluorescence imaging with near-infrared light: new technological advances that enable *in vivo* molecular imaging. Eur Radiol 2003;13:195 – 208.

31. Ntziachristos V, Ripoll J, Wang LV, Weissleder R. Looking and listening to light: the evolution of whole-body photonic imaging. Nat Biotechnol 2005;23:313 – 20.

32. Weissleder R, Tung CH, Mahmood U, Bogdanov A, Jr. *In vivo* imaging of tumors with protease-activated near-infrared fluorescent probes. Nat Biotechnol 1999;17:375 – 8.

33. Ke S, Wen X, Gurfinkel M, et al. Near-infrared optical imaging of epidermal growth factor receptor in breast cancer xenografts. Cancer Res 2003;63:7870 – 5.

34. Song A, Wang X, Zhang J, Marik J, Lebrilla CB, Lam KS. Synthesis of hydrophilic and flexible linkers for peptide derivatization in solid phase. Bioorg Med Chem Lett 2004;14:161 – 5.

35. Aina OH, Sroka TC, Chen ML, Lam KS. Therapeutic Cancer Targeting Peptides. Biopolymers 2002;66:184 – 99.

36. Aina OH, Marik J, Liu R, Lau DH, Lam KS. Identification of novel targeting peptides for human ovarian cancer cells using ''one-bead one-compound'' combinatorial libraries. Mol Cancer Ther 2005;4:806 – 13.

37. Aina OH, Marik J, Gandour-Edwards R, Lam KS. Near-infrared optical imaging of ovarian cancer xenografts with novel $\alpha3$-integrin binding peptide ''OA02.'' Mol Imaging 2005;4:439 – 47.

38. Lau D, Guo L, Liu R, Marik J, Lam KS. Peptide ligands targeting integrin $\alpha3\beta1$ in non-small cell lung cancer. Lung Cancer 2006;52: 291 – 7.